SIGNAL TRANSDUCTION

Oscillatory stress stimulation uncovers an Achilles' heel of the yeast MAPK signaling network

Amir Mitchell,[1,2] Ping Wei,[1,3]* Wendell A. Lim[1,2,4]*

Cells must interpret environmental information that often changes over time. In our experiment, we systematically monitored the growth of yeast cells under various frequencies of oscillating osmotic stress. Growth was severely inhibited at a particular resonance frequency, at which cells show hyperactivated transcriptional stress responses. This behavior represents a sensory misperception: The cells incorrectly interpret oscillations as a staircase of ever-increasing osmolarity. The misperception results from the capacity of the osmolarity-sensing mitogen-activated protein kinase (MAPK) network to retrigger with sequential osmotic stresses. Although this feature is critical for coping with natural challenges, such as continually increasing osmolarity, it results in a trade-off of fragility to non-natural oscillatory inputs that match the retriggering time. These findings demonstrate the value of non-natural dynamic perturbations in exposing hidden sensitivities of cellular regulatory networks.

Cells have evolved complex signaling networks to monitor and respond to stimuli in their environment. As the cellular environment can dynamically change, evolution may select for sensory systems that are optimized for temporal patterns of stimulation that are frequently encountered by the organism. Such sensory systems may perform poorly when challenged by a non-natural stimulus pattern. Thus, exposing cells to time-variant inputs in controlled experiments can shed light on the mechanisms underlying cellular response, as well as the selection forces that shaped the biological system during evolution.

We systematically probed how the fitness of yeast cells responded to different dynamic patterns of osmotic stress. In *Saccharomyces cerevisiae*, the Hog1 mitogen-activated protein kinase (MAPK) pathway responds to increases in osmotic stress and ultimately leads to increased synthesis and retention of glycerol (*1*). Activation of the Hog1 MAPK is transient, even when osmotic stress persists (*2*). This adaptation allows cells to reset themselves and remain responsive to further increasing osmolarity that might occur with evaporation (*3*). Although MAPK signaling dynamics are well characterized, relatively little is known about the fitness of yeast cells when faced with different dynamic patterns of osmolarity.

We used time-lapse microscopy with single-cell resolution to monitor cell growth under dynamically controlled osmolarity profiles (Fig. 1A and supplementary materials and methods). Cells grown in microfluidic chambers were subjected to regular oscillations in osmolarity over a time span allowing for multiple rounds of cell division (amplitude range: 0 to 0.4 M KCl). We tracked colony growth when cells were exposed to continuous high osmolality (single-step increase) or to oscillations in osmolarity with a periodicity of 1, 8, or 32 min (Fig. 1B). Although the integrated osmolarity experienced by cells during these experiments was identical, cells grew considerably slower under the intermediate frequency of 8 min (movie S1). When tested under a wide range of oscillatory frequencies (0.5 to 128 min), cellular growth was drastically hampered in a

[1]Department of Cellular and Molecular Pharmacology, University of California, San Francisco (UCSF), San Francisco, CA 94158, USA. [2]Center for Systems and Synthetic Biology, UCSF, San Francisco, CA 94158, USA. [3]Center for Quantitative Biology, and Peking-Tsinghua Center for Life Sciences, Academy for Advanced Interdisciplinary Studies, School of Life Sciences, Peking University, Beijing 100871, China. [4]Howard Hughes Medical Institute (HHMI), UCSF, San Francisco, CA 94158, USA.
*Corresponding author. E-mail: lim@cmp.ucsf.edu (W.A.L.); pwei@pku.edu.cn (P.W.)

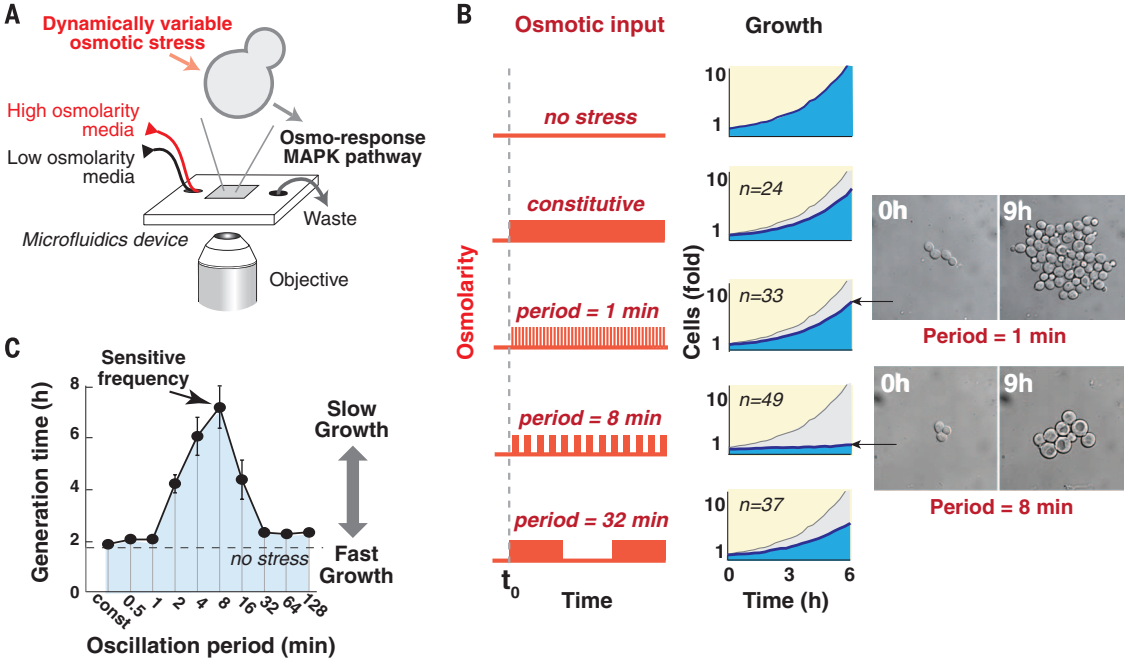

Fig. 1. Osmotic oscillations at an intermediate frequency cause slow proliferation. (**A**) Schematic of the flow chamber used in our experiment. (**B**) Cell growth under various frequencies of mild osmostress (0.4 M KCl). The graphs show the average number of progeny cells relative to the number of cells before stress is applied (*n* indicates the number of parental cells monitored). Growth without osmotic stress is depicted in gray. The insets at right show representative images of cells. (**C**) Systematic frequency scan of mild osmotic oscillations (0.4 M KCl). The graph shows the mean doubling time over a period of 8 hours. Each point marks the mean generation time calculated from at least 50 individual sets of progeny in two biological repeats. Error bars indicate SE.

narrow range of intermediate frequencies, with this inhibitory effect peaking at an 8-min resonance frequency (Fig. 1C). At this periodicity, cells were larger and contained large vacuoles (fig. S2).

To explore what cellular mechanisms might underlie the band-pass frequency selectivity of growth inhibition, we used a computational model developed to study the adaptive dynamics of yeast osmotic signaling (*3*) (Fig. 2A). Changes in the turgor pressure across the cell wall and membrane are sensed and culminate in phosphorylation of the MAPK Hog1. Phosphorylated Hog1 (Hog1-PP) regulates cytoplasmic proteins and gene expression, thus increasing internal glycerol concentrations and restoring turgor pressure. In response to a single-step osmotic shock, accumulation of Hog1-PP shows two phases: an induction phase that quickly peaks at 5 min, followed by slower adaptation within 30 min (Fig. 2B). However, if osmolarity stress is suddenly removed, Hog1-PP levels decrease almost immediately through action of protein phosphatases.

Because downstream changes in Hog1-PP–induced gene expression are expected to occur on a much slower time scale (hours) (*4*) as compared with MAPK adaptation (minutes), we can use the integral under the Hog1-PP curve as an approximation for the expected level of downstream transcriptional output (Fig. 2B). In response to a single-step increase in osmolarity, Hog1-PP shows a transient adaptive curve, and transcriptional output is expected to monotonically increase and reach a plateau once Hog1-PP returns to its basal level (protein levels will slowly decay afterward due to dilution and degradation). Similar downstream dynamics are not restricted to transcription but can manifest in any cellular activity that involves slow decay and hence acts as an integrator of MAPK signaling activity over time.

By tracking expected changes in osmotic stress–induced gene expression, this computational model can explain the stress sensitivity at the resonance frequency. We used the model to estimate response

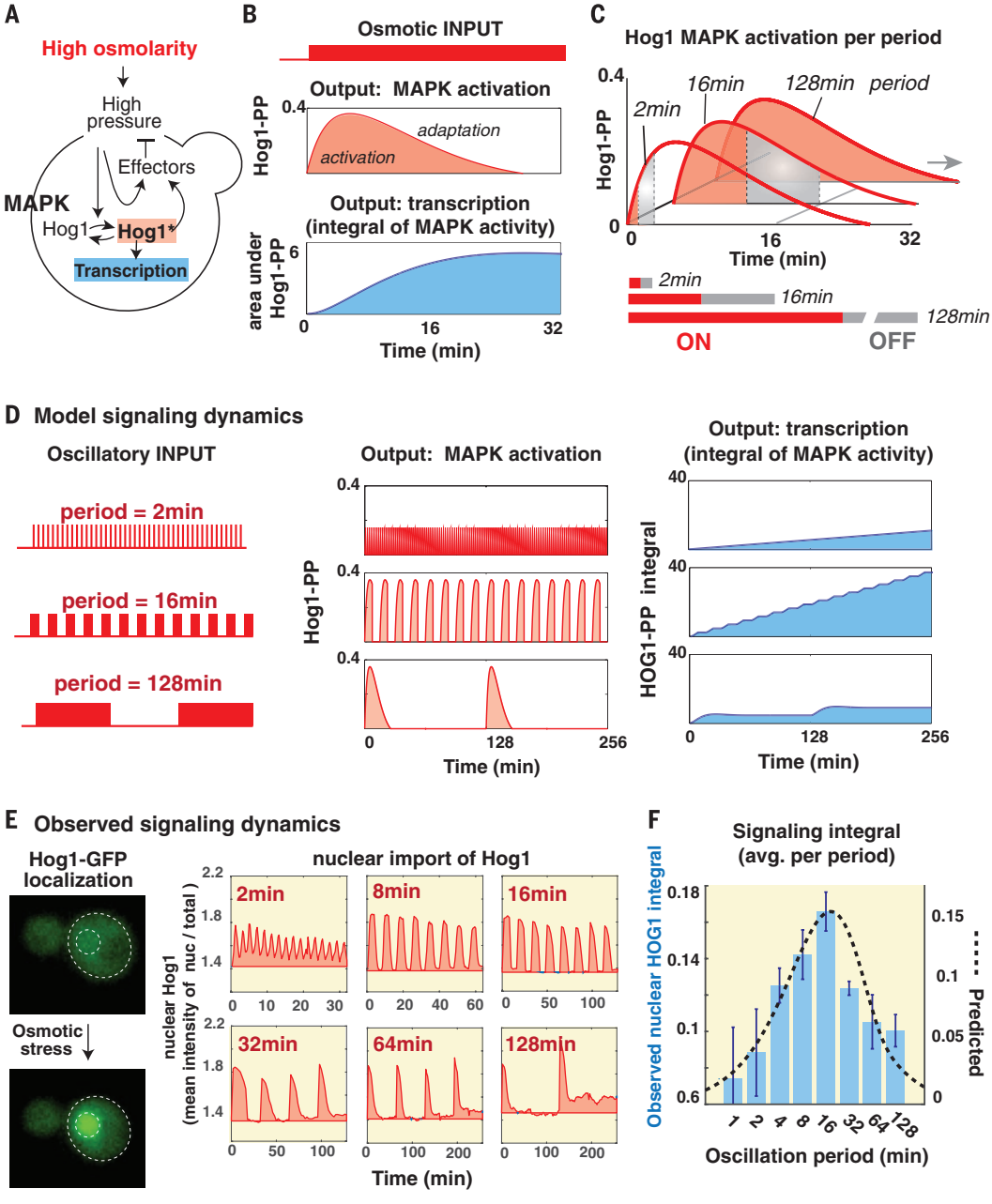

Fig. 2. Mathematical modeling of adaptive signaling of the osmotic pathway predicts downstream pathway hyperactivation at resonance stress frequency. (**A**) Schematic of the osmotic pathway (*3*). Changes in turgor pressure activate Hog1-dependent and Hog1-independent response arms that act to reduce deviation from the optimal turgor pressure. (**B**) Pathway activation according to the perfect-adaptation model (*3*). (Top) Predicted amounts of Hog1 phosphorylation in response to a 0.4 M increase in osmolality with induction and adaptation phases. (Bottom) Integral under the Hog1-PP curve, taken as an approximation of the accumulated transcriptional output. (**C**) Pathway activation at three representative pulse durations (ON and OFF intervals are marked in red and gray, respectively). The area under the predicted signaling curve (Top) was normalized to the entire pulse period (ON + OFF) (Bottom). (**D**) Model-predicted signaling and transcriptional dynamics under representative oscillation periods. (**E**) Experimentally observed signaling dynamics under representative oscillation periods, as measured by tracking Hog1-GFP nuclear localization. The graphs show the mean intensity ratio of nuclear Hog1-GFP over total Hog1-GFP in 40 to 100 cells (relative to the basal ratio at t = 0 min). (**F**) Measured signaling integral (normalized per minute) in a frequency scan. The blue bars show the average integral in two biological repeats (error bars indicate SD). The dashed black curve marks the model predictions.

dynamics for a cell exposed to a high-osmolarity pulse at three representative pulse durations (Fig. 2C). Under oscillations, the ON pulse is followed by an OFF pulse of the same length; therefore, the averaged transcriptional rate can be calculated from the integral under the signaling curve divided by the length of the full pulse period (ON + OFF duration). The model predicts that the normalized transcriptional output will maximize at an intermediate frequency of 16 min (as though the system contains a band-pass filter). The signaling dynamics have markedly different effects at different frequencies (Fig. 2D): Under a high-frequency stimulus, the signaling is terminated quickly, leading to very slow transcription. However, under an intermediate frequency, the signaling peaks in each oscillation. Because oscillations are still relatively frequent, signaling results in a high, ever-increasing transcriptional output. Under a low frequency, the signaling peaks and completely adapts. Yet because the encounters with stress are rare, this leads to a low overall transcriptional output. We experimentally tested this hypothesis by tracking Hog1–green fluorescent protein (GFP) localization under osmotic oscillations as a proxy for signaling dynamics (Hog1-GFP enters the nucleus when activated) (Fig. 2E). We observed a good agreement with the model predictions: The integral under the nuclear Hog1-GFP curve is maximized for an intermediate frequency of 16 min (Fig. 2F).

Thus, the model points to a plausible cellular mechanism: Adaptive signaling dynamics (the ability of the MAPK to reset and retrigger) may lead to downstream pathway hyperactivation at an intermediate resonance frequency. We used live-cell reporters (promoters linked to fluorescent proteins) to examine the transcriptional activity of the osmotic pathway and the intimately related invasive growth MAPK pathway that is triggered by starvation (Fig. 3A) (*5*, *6*). Note that despite sharing many common components, the individual pathways normally remain highly insulated from one another (*5*, *7*–*11*). Under a single-step osmotic stress, cells transiently induced the osmotic transcriptional response (peaking at 50-fold after 2 hours) (movie S1) with very little effect on the invasive-growth pathway (Fig. 3B). However, oscillatory osmolarity led to continuous induction of the osmotic response, culminating in pathway hyperactivation (450-fold increase after 8 hours) (movie S1). Moreover, the oscillations also led to full activation of the normally isolated invasive pathway (consistent with morphological changes observed for some cells) (fig. S2). A frequency scan showed that transcription of both pathways peaks at an intermediate frequency range (8 to 16 min) (Fig. 3C). The mating pathway, a third interwoven pathway, remains isolated (fig. S3) (*10*, *12*). Thus, stimulation at the resonance frequency led to hyperactivation of the osmotic response and misactivation of the invasive growth response (Fig. 3D).

To evaluate whether both osmotic hyperactivation and cross-talk with the invasive pathway

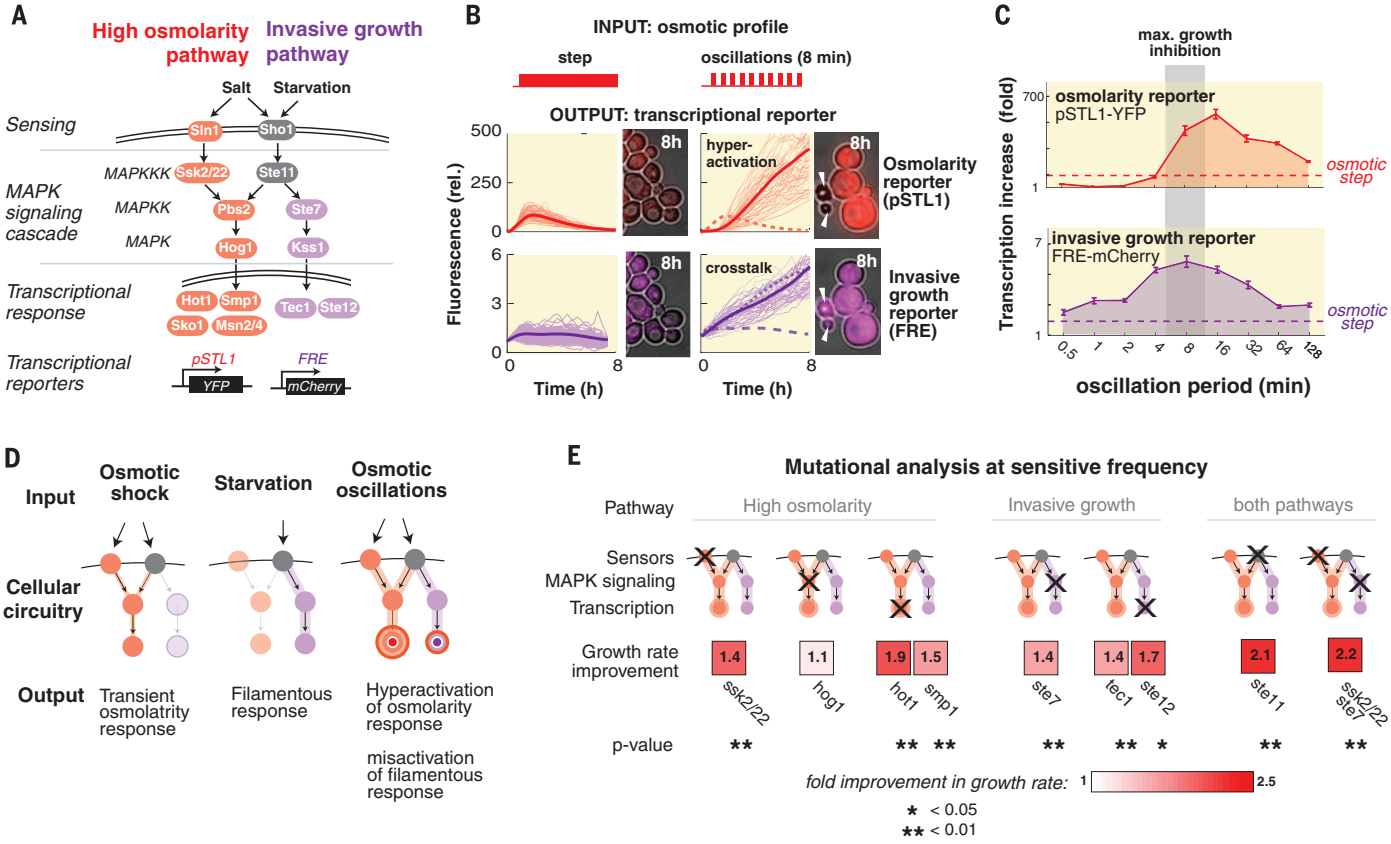

Fig. 3. Pathway hyperactivation and cross-talk underlie growth inhibition at the sensitive frequency. (**A**) Network diagram of the high-osmolality and invasive-growth pathways. YFP, yellow fluorescent protein. (**B**) Transcriptional output of the pathways in response to alternative inputs. The graphs show the mean fold induction in florescence per cell and the single-cell traces of cells within the interquartile range. The graph with the dotted purple line shows full pathway activation in response to butanol. Although pathway isolation is maintained under a step input profile, osmotic oscillations lead to hyperactivation of the osmotic response and full activation of the invasive-growth pathway. The microscopy images show representative cells 8 hours after their first exposure to stress. Arrowheads indicate cells that died during the stress period. (**C**) Transcriptional response at various frequencies of osmotic stress (0.4 M KCl). The activity of both reporters behaves as a band-pass filter, with peaked activity at intermediate frequencies (8 to 16 min). Error bars indicate SE of maximal fold fluorescence measured for 70 to 200 individual cells. (**D**) Frequency-dependent model of the MAPK network that explains growth inhibition at the resonance frequency. (**E**) Mutational analysis points to a contribution from both pathways in growth inhibition under osmotic oscillations (0.4 M, 8-min period). The color code marks the fold improvement of the deleted strain relative to the WT strain. Statistical significance was evaluated with the *t* test (comparing the mean growth rate of multiple progeny of the deleted strain and multiple progeny of the cocultured WT strain).

are detrimental to growth, we tested the phenotypes of specific mutations. We reasoned that deletions that weaken pathway activity might improve growth under oscillatory osmotic stress (Fig. 3E and fig. S5). Our measurements indicated that weakening the pathway by deletion of one of the osmosensing branches improved growth (complete knockout of the osmotic pathway did not improve growth because the core protective osmotic response is still necessary, even under oscillations). We also observed that knockout of invasive pathway genes is beneficial and that deletions targeting shared components in both pathways, such as Ste11 MAPK kinase kinase (*13*), are more advantageous than deletions targeting only one pathway.

Given the detrimental effects of pathway hyperactivation, we reasoned that an improved cascade could be engineered by adding a slow negative-feedback loop to the MAPK cascade. Ideally, this feedback would allow an initial osmotic response while dampening rapid retriggering (adding a longer refractory period). We implemented a feedback loop using OspF, a previously characterized bacterial effector protein that irreversibility inactivates phosphorylated Hog1 (*14*) (Fig. 4A). Monitoring the transcription in an engineered strain showed that the engineered pathway is still responsive to a single-step input but is not hyperactivated under oscillations (Fig. 4B and movie S2).

We then tested whether this network rewiring could improve growth under alternative dynamic stress inputs (Fig. 4C). Consistent with measurements of transcriptional activity, we observed that the engineered and wild-type (WT) strains had equal growth rates when exposed to a single step of osmotic stress but that the engineered negative-feedback strain grew considerably faster under osmotic oscillations. Nonetheless, when we compared strain growth under more natural types of dynamic stress profiles, we observed an opposite trend: Under a primed or gradually increasing osmolarity pattern, as may occur during evaporation of an aqueous niche, the WT strain grew faster. Thus, there is an inherent trade-off—our rewiring prevents detrimental pathway hyperactivation in response to oscillations but also leads to impaired growth in dynamic environments that truly require pathway reactivation (such as naturally occurring upward ramps of stress).

The detrimental sensitivity to osmotic oscillations can be viewed as an inherent limitation of the underlying biological system (Fig. 4D). In analogy to a sensory misperception phenomenon, the ability of oscillations to retrigger the osmotic response is misinterpreted by the cells as an infinite staircase increase in osmolality (*15*) that culminates in deleterious transcriptional hyperactivation. Thus, although the adaptive response allows the biological system to remain responsive in complex environments that it experiences in nature, it also creates an inherent "Achilles' heel" due to its failure to prevent pathway hyperactivation in non-natural oscillating environments. From an evolutionary perspective, this Achilles' heel is unimportant because the yeast are unlikely to experience oscillatory stress at the resonant frequency.

Our observations in yeast may have implications for the dynamic sensitivities of other biological systems, as many responses display adaptation or the ability to retrigger (*16*), and these may also have resonance frequency sensitivities. Our results may additionally be relevant for cellular signaling in disease, as mutations affecting cellular signaling are common in cancer, autoimmune disease, and diabetes. These mutations may rewire the native network and thus could modify its activation and adaptation dynamics. Such network rewiring in disease may lead to changes that can be most clearly revealed by simulation with oscillatory inputs or other non-natural patterns. The changes in network response behaviors could be exploited for diagnosis and functional profiling of disease cells or could potentially be taken advantage of as an Achilles' heel to

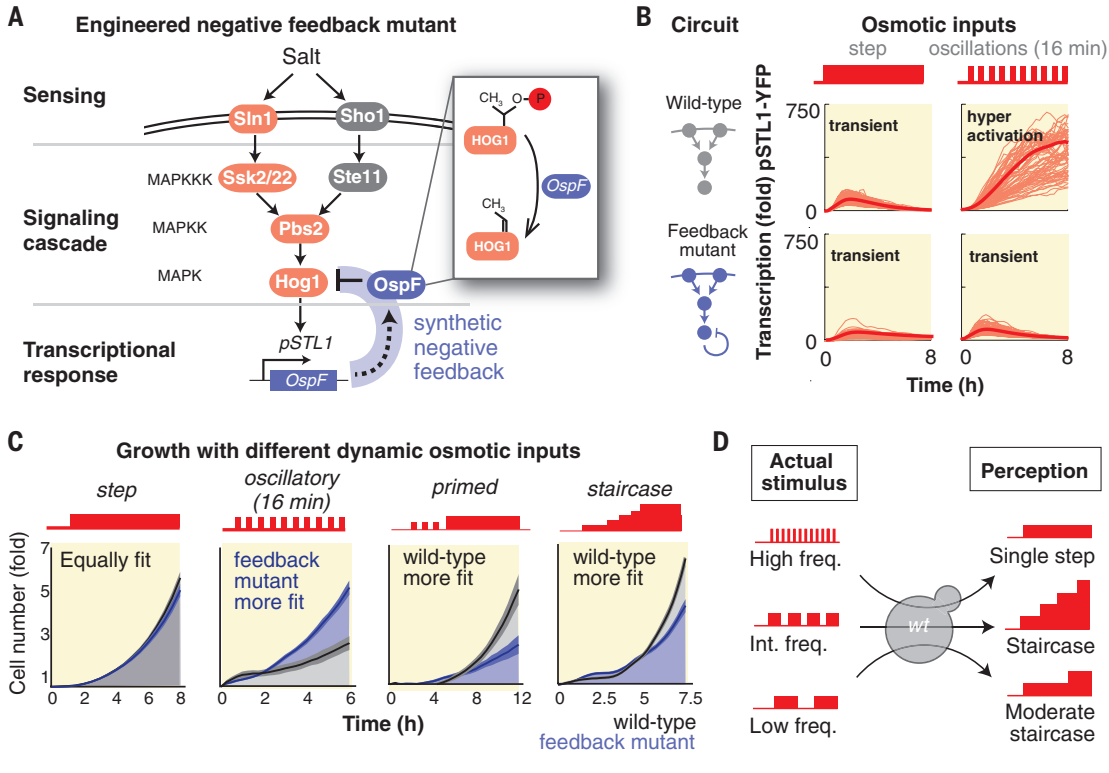

Fig. 4. Introducing a synthetic feedback loop resolves osmotic hyperactivation and relieves growth inhibition under osmotic oscillations but also reduces proliferation under more natural input dynamics. (**A**) Diagram of the genetic circuit that underlies the conditional negative feedback. The bacterial effector OspF (fused to an osmotic stress–responsive promoter) deactivates phosphorylated Hog1 by removing a hydroxyl group (*14*), leading to a longer delay in retriggering of the pathway. (**B**) Transcriptional response of the osmotic pathway in the WT strain and engineered strain. Both strains show a transient response after an osmotic shock but respond differently to an oscillating input. The graphs show the mean fold induction in florescence per cell and the single-cell traces of cells within the interquartile range. (**C**) Comparative growth assays of the WT and engineered strains under alternative inputs. (**D**) Growth inhibition under oscillatory input originates from the adaptive nature of the osmotic response. Although the signaling cascade effectively filters oscillatory inputs at a high frequency (*15*), oscillations at a lower frequency lead to repeated stimulation of the osmotic pathway. In this frequency range, the cascade circuitry perceives an oscillatory input as gradually increasing osmolarity and hence keeps the osmotic pathway continuously active to counteract the seemingly increasing high osmolality. Growth inhibition is maximized at an intermediate frequency because it is interpreted as the steepest stepwise (i.e., staircase) increase in osmolality, which leads to peaked levels of downstream hyperactivation.

selectively target cells bearing the diseased network (*17*).

REFERENCES AND NOTES

1. H. Saito, F. Posas, *Genetics* **192**, 289–318 (2012).
2. J. L. Brewster, T. de Valoir, N. D. Dwyer, E. Winter, M. C. Gustin, *Science* **259**, 1760–1763 (1993).
3. D. Muzzey, C. A. Gómez-Uribe, J. T. Mettetal, A. van Oudenaarden, *Cell* **138**, 160–171 (2009).
4. U. Alon, *An Introduction to Systems Biology: Design Principles of Biological Circuits* (Chapman & Hall/CRC, 2006).
5. H. D. Madhani, G. R. Fink, *Science* **275**, 1314–1317 (1997).
6. K. Furukawa, S. Hohmann, *Mol. Microbiol.* **88**, 5–19 (2013).
7. M. C. Good, J. G. Zalatan, W. A. Lim, *Science* **332**, 680–686 (2011).
8. M. Good, G. Tang, J. Singleton, A. Reményi, W. A. Lim, *Cell* **136**, 1085–1097 (2009).
9. H. D. Madhani, C. A. Styles, G. R. Fink, *Cell* **91**, 673–684 (1997).
10. S. M. O'Rourke, I. Herskowitz, *Genes Dev.* **12**, 2874–2886 (1998).
11. E. A. Elion, *J. Cell Sci.* **114**, 3967–3978 (2001).
12. J. G. Zalatan, S. M. Coyle, S. Rajan, S. S. Sidhu, W. A. Lim, *Science* **337**, 1218–1222 (2012).
13. F. Posas, H. Saito, *Science* **276**, 1702–1705 (1997).
14. P. Wei *et al*., *Nature* **488**, 384–388 (2012).
15. P. Hersen, M. N. McClean, L. Mahadevan, S. Ramanathan, *Proc. Natl. Acad. Sci. U.S.A.* **105**, 7165–7170 (2008).
16. J. E. Purvis, G. Lahav, *Cell* **152**, 945–956 (2013).
17. M. Behar, D. Barken, S. L. Werner, A. Hoffmann, *Cell* **155**, 448–461 (2013).

ACKNOWLEDGMENTS

We thank H. Youk, R. Almeida, S. Coyle, and M. Thomson for insightful discussions. This work was supported by NIH grants R01 GM55040, R01 GM62583, PN2 EY016546, and P50 GM081879; the NSF Synthetic Biology Engineering Research Center (SynBERC); and HHMI (to W.A.L.). This work was also supported in part by MOST grant 2015CB910300, National Natural Science Foundation of China grant 31470819, and Peking-Tsinghua Center for Life Sciences (to P.W.). A.M. is a European Molecular Biology Organization Fellow (ALTF 419-2010) and the recipient of a Program for Breakthrough Biomedical Research Postdoctoral Research Award (UCSF).

SUPPLEMENTARY MATERIALS

www.sciencemag.org/content/350/6266/1379/suppl/DC1
Materials and Methods
Figs. S1 to S5
Tables S1 and S2
References (*18*, *19*)
Movies S1 and S2

10 March 2015; accepted 8 November 2015
Published online 19 November 2015
10.1126/science.aab0892

TRANSCRIPTION

RNA polymerase II–associated factor 1 regulates the release and phosphorylation of paused RNA polymerase II

Ming Yu,[1]* Wenjing Yang,[2]* Ting Ni,[3] Zhanyun Tang,[1] Tomoyoshi Nakadai,[1] Jun Zhu,[2] Robert G. Roeder[1]†

Release of promoter-proximal paused RNA polymerase II (Pol II) during early elongation is a critical step in transcriptional regulation in metazoan cells. Paused Pol II release is thought to require the kinase activity of cyclin-dependent kinase 9 (CDK9) for the phosphorylation of DRB sensitivity–inducing factor, negative elongation factor, and C-terminal domain (CTD) serine-2 of Pol II. We found that Pol II–associated factor 1 (PAF1) is a critical regulator of paused Pol II release, that positive transcription elongation factor b (P-TEFb) directly regulates the initial recruitment of PAF1 complex (PAF1C) to genes, and that the subsequent recruitment of CDK12 is dependent on PAF1C. These findings reveal cooperativity among P-TEFb, PAF1C, and CDK12 in pausing release and Pol II CTD phosphorylation.

Thousands of developmentally regulated genes in metazoans harbor promoter-proximal paused RNA polymerase II (Pol II) 30 to 50 nucleotides downstream of their transcription start sites (TSS) (*1*–*3*). Paused Pol IIs are usually phosphorylated on C-terminal domain (CTD) Ser^5 and are associated with 5,6-dichloro-1-β-D-ribofuranosylbenzimidazole (DRB) sensitivity–inducing factor (DSIF) and negative elongation factor (NELF). Release of paused Pol II into productive elongation is believed to require phosphorylation of CTD Ser^2, conversion of DSIF into a positive elongation factor by phosphorylation of its SPT5 subunit, and disassociation of NELF (*1*). Although it was long believed that CTD Ser^2 phosphorylation was catalyzed predominantly by cyclin-dependent kinase 9 (CDK9), the mammalian ortholog of yeast Bur1, recent studies have identified CDK12 as the metazoan ortholog of Ctk1, the major CTD Ser^2 kinase in yeast, and suggested that CDK9 is a CTD Ser^5 kinase (*4*, *5*). The yeast Paf1 complex and the human PAF1 complex, of interest here, have been implicated in transcription elongation on DNA and chromatin templates, recruitment and activation of histone modifiers, mRNA 3′ formation, etc. (*6*, *7*). However, PAF1C has not been considered a critical elongation factor because depletions of PAF1C subunits in yeast and fly, while reducing the level of CTD Ser^2-phosphorylated elongating Pol II (*8*, *9*), did not affect the distribution of total Pol II on active genes (*8*, *10*).

To study the function of human PAF1C, we performed chromatin immunoprecipitation sequencing (ChIP-seq) experiments for PAF1C subunits PAF1, CDC73, LEO1, and CTR9, as well as total Pol II and CTD Ser^2-phosphorylated Pol II [Pol II (ser-2p)], in human acute myeloid leukemia THP1 cells. Similar to Pol II (ser-2p), the four PAF1C subunits occupied transcribed regions of most active genes and exhibited maximum occupancy downstream of transcription end sites (TESs) (Fig. 1, A to C, and fig. S1, A to F). LEO1 (fig. S1B) and CTR9 (fig. S1C) occupancies did not generally overlap with the promoter-proximal Pol II peaks, as reported previously (*2*). However, PAF1 and CDC73, the major scaffolding components within human PAF1C (*11*), did overlap with the promoter-proximal Pol II peaks (Fig. 1, B and C, and fig. S1, A, D, E, and F). Complementary strand-specific mRNA-seq analyses using RNA from THP1 cells identified 19,481 transcripts [reads per kilobase of transcript per million mapped reads (RPKM) > 1], corresponding to 10,664 genes, of which 9823 were bound by PAF1. Notably, the PAF1 binding signals on these genes positively correlated with corresponding mRNA levels (Fig. 1C and fig. S1, A to C), suggesting an involvement of PAF1C in Pol II transcription or transcription-coupled events.

In further functional analyses, we used two lentiviral short hairpin RNAs (shRNA #1 and shRNA #2, targeting different regions of the *PAF1*mRNA) to reduce the level of the key PAF1 subunit (*8*, *11*) in THP1 cells (Fig. 2A) and assessed global gene expression changes by RNA-seq. With false discovery rate < 0.01 and considering only relative expression change by a factor of >1.5, of the 9823 genes bound by PAF1, only 1351 showed changes in expression (table S1). The knockdown of PAF1 also resulted in an increased level of promoter-proximal paused Pol II that was not limited to genes whose mRNA levels were affected by PAF1 knockdown (Fig. 2, B and C). Considering only genes with a normalized promoter read count change of >2, 5851 exhibited increased Pol II pausing and only 344 exhibited

[1]Laboratory of Biochemistry and Molecular Biology, The Rockefeller University, New York, NY 10065, USA. [2]Systems Biology Center, National Heart, Lung, and Blood Institute, Bethesda, MD 20892, USA. [3]State Key Laboratory of Genetic Engineering and Ministry of Education Key Laboratory of Contemporary Anthropology, Collaborative Innovation Center of Genetics and Development, School of Life Sciences, Fudan University, Shanghai 200438, P.R. China.
*These authors contributed equally to this work. †Corresponding author. E-mail: roeder@rockefeller.edu